Coexistence of superconductivity and antiferromagnetic ordering in the layered superconductor SmFePO

Yoichi Kamihara,[1,*] Hidenori Hiramatsu,[1] Masahiro Hirano,[1,2] Yasuhiro Kobayashi,[3,4] Shinji Kitao,[3,4] Satoshi Higashitaniguchi,[3,4] Yoshitaka Yoda,[4,5] Makoto Seto,[3,4,6] and Hideo Hosono[1,2,7]

[1]*ERATO-SORST, JST, Frontier Research Center, Tokyo Institute of Technology, Mail Box S2-13, 4259 Nagatsuta, Midori-ku, Yokohama 226-8503, Japan*

[2]*Frontier Research Center, Tokyo Institute of Technology, Mail Box S2-13, 4259 Nagatsuta, Midori-ku, Yokohama 226-8503, Japan*

[3]*Research Reactor Institute, Kyoto University, Kumatori-cho, Sennan-gun, Osaka 590-0494, Japan*

[4]*CREST, JST, Honcho, Kawaguchi, Saitama 332-0012, Japan*

[5]*Japan Synchrotron Radiation Research Institute, 1-1-1 Kouto, Mikazuki-cho, Sayo-gun, Hyogo 679-5198, Japan*

[6]*Japan Atomic Energy Agency, 1-1-1 Koto, Sayo-cho, Sayo-gun, Hyogo 679-5148, Japan*

[7]*Materials and Structures Laboratory, Tokyo Institute of Technology, Mail Box R3-1, 4259 Nagatsuta, Midori-ku, Yokohama 226-8503, Japan*

(Received 1 October 2008; published 18 November 2008)

Superconductivity and magnetic transition in SmFePO were examined by electric, magnetic, ^{57}Fe Mössbauer, and ^{149}Sm nuclear resonant forward-scattering (NRFS) measurements. Zero resistivity and negative magnetic susceptibility were observed in an undoped SmFePO, indicating superconducting transition temperature (T_c) of ~3 K. T_c in undoped SmFePO appears in a narrow region of lattice constants with an optimum conductivity. Furthermore, in relation to magnetic susceptibility, NRFS spectra verify that magnetic moments of Sm^{3+} ions order antiferromagnetically below magnetic transition ~5 K, accompanying a discontinuous drop in electrical resistivity, whereas ^{57}Fe Mössbauer spectra show that magnetic moments of Fe are quenched. These results indicate the coexistence of superconductivity and magnetic ordering in a crystallographic unit cell of SmFePO.

DOI: 10.1103/PhysRevB.78.184512 PACS number(s): 74.25.Fy, 74.25.Ha, 74.25.Jb, 79.60.−i

I. INTRODUCTION

In conventional superconductors, magnetic impurities at a level of ~1 at %, which partially occupy specific crystallographic sites, strongly suppress superconductivity.[1] Therefore, exceptional superconducting compounds whose specific crystallographic sites are occupied by magnetic elements [$LnMo_6S_8$ (Ln=Gd,Tb,Dy,Ho,Er) (Refs. 2 and 3) and $LnRh_4B_4$ (Ln=Nd,Sm,Er,Tm) (Refs. 2 and 4)] were called exotic or "magnetic superconductors" for several decades. However, a considerable number of magnetic superconductors[5,6] have been found, including high-T_c superconductor $LnBa_2Cu_3O_{7-\delta}$ (Ln=Y,La,Nd,Sm,Eu,Gd,Ho,Er,Lu) (Ref. 7) and electron-doped high-T_c superconductor $Ln_{2-x}Ce_xCuO_4$ (Ln=Pr,Nd,Sm).[8] The recently found high-T_c superconductor family of F-doped LnFePnO (Ln=La,Ce,Pr,Nd,Sm,Gd,Tb,Pn=P,As) (Refs. 9–16) is considered to be a member of this category because antiferromagnetic ordering of magnetic moments of rare-earth ions is reported for superconducting F-doped LnFeAsO (Ln=Ce,Nd,Sm).[17] The crystals have a common layered structure belonging to the tetragonal $P4/nmm$ space group and are composed of an alternate stack of LnO and FePn layers (Fig. 1). The FePn layer contributes to a dominant carrier conduction path, whereas the LnO layer acts as a carrier blocking layer.[18] The undoped LnFeAsO shows a phase transition from tetragonal to orthorhombic phase at ~160 K.[19] The transition probably correlates with the antiferromagnetic ordering of iron because both the crystallographic and magnetic transitions vanish with the emergence of superconductivity.[20] On the other hand, although a finite magnetic interaction exists between carriers and the magnetic moments of Ln ions, it does not affect T_c.[21] Further, such relationships between magnetism and T_c are not reported for LnFePO.

In this study, we examine superconducting and magnetic properties of SmFePO based on electrical and magnetic measurements as well as conventional Mössbauer spectroscopy (MS) (Ref. 22) and nuclear resonant forward-scattering (NRFS) spectroscopy.[23,24] The MS and NRFS spectroscopies are sufficiently sensitive to examine the state of ^{57}Fe and ^{149}Sm nuclei, making it possible to measure internal mag-

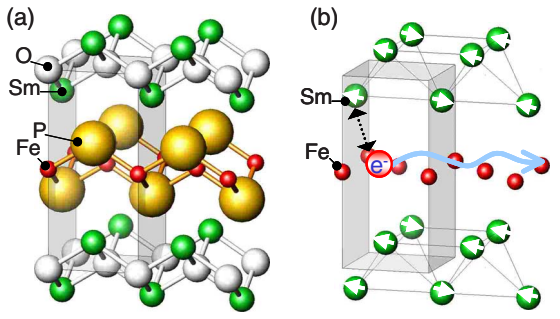

FIG. 1. (Color online) (a) Crystal structure of SmFePO. The light blue box represents the unit cell. FeP_4 units are shown as gray tetrahedra. (b) Schematic electrical conduction in SmFePO. Conducting carriers (probably electrons) mainly flow in the tetragonal sublattice built by Fe. Sm ions have a localized magnetic moment (represented by arrows). A finite magnetic interaction indicated by a slashed arrow exists between carriers and the magnetic moments of Ln ions.

netic fields (H_{int}) acting on both nuclei independently. Therefore, we can obtain the site-specific magnetic states of Fe and Sm with certainty. Furthermore, it is of interest whether the low T_c of undoped LaFePO (2.4–5.5 K) (Ref. 25) increases or not by substituting Sm^{3+} at the La^{3+} ion sites. We also analyze possible factors affecting the observed scatter in T_c including electrical resistivity and lattice constants.

II. EXPERIMENT

Polycrystalline samples were prepared by solid-state reactions using dehydrated Sm_2O_3 and a mixture of compounds composed of SmP, Fe_2P, and FeP (SmP-Fe_2P-FeP powder) as starting materials. The dehydrated Sm_2O_3 was prepared by heating commercial Sm_2O_3 powder (Kojundo Chemical; 99.9%) at 1000 °C for 5 h in air. To obtain the mixture of compounds, Sm (Nilaco; Sm with purity 99.9%), Fe (Kojundo Chemical; >99.9%), and P (Rare Metallic Chemical; 99.999%) were mixed in a ratio of 1:3:3 and heated at 700 °C for 10 h in an evacuated silica tube. Then, a 1:1 mixture of the two compound powders was heated in an evacuated silica tube at 1200 °C for 40 h to prepare a sintered pellet. To prevent a collapse of the silica tube used in the reaction, the tube was filled with high-purity Ar gas with a pressure of 0.2 at room temperature.

The phase purity, lattice constants, and crystal structure of the sintered powders were examined by powder x-ray diffraction (XRD) (Bruker D8 Advance TXS) using Cu Kα radiation from a rotating anode with the help of the Rietveld refinement using Code TOPAS3.12.[26] dc electrical resistivity (ρ) was measured by a four-probe technique using a Au electrode at temperatures from 1.8 to 300 K. Magnetization measurements were performed with a vibrating sample magnetometer (Quantum Design) in the same temperature range. ^{57}Fe Mössbauer spectroscopy was performed at temperatures from 2.2 to 298 K. NRFS spectra were taken at the BL09XU beamline of SPring-8. The storage ring was operated in a 203-bunch mode, providing a bunch distance of 23.6 ns. Undulator radiation was monochromatized to the bandwidth of 1.5 meV (full width at half maximum) with a high-resolution monochromator consisting of asymmetric Si (4 4 0) and Si (16 8 8) at the nuclear resonance energy (22.507 keV) of ^{149}Sm. NRFS was measured using a multielement avalanche photodiode detector. A time-delayed component of ^{149}Sm NRFS, monitored at times from 3 to 16 ns, was measured at temperatures from 3 to 180 K. Time spectra of ^{149}Sm NRFS were measured at 3 and 150 K. The MOTIF package was used for the analysis of the NRFS data.[27]

III. RESULTS

A. Structural characterization

Figure 2 shows a representative powder XRD pattern of SmFePO. Almost all the diffraction peaks are assigned to those of the SmFePO phase, indicating that the sample is composed of almost a single SmFePO phase, although there are several minor peaks attributable to normal conducting FeP, Fe_2P, and insulating Sm_2O_3 (indicated by the positions of the Bragg diffractions in the figure).[28–30] Lattice constants

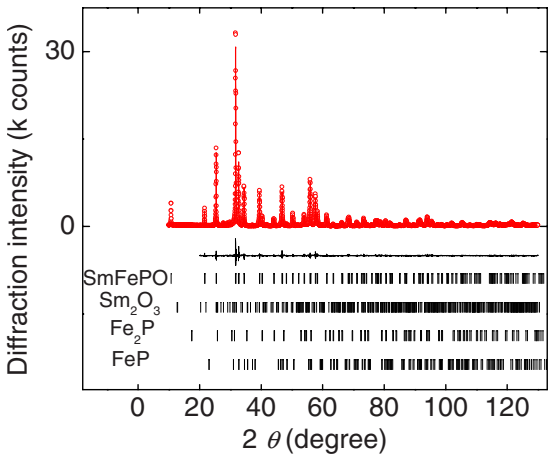

FIG. 2. (Color online) XRD patterns of SmFePO observed (red circles) and simulated by Rietveld analysis (red line). The black line represents the difference between the two. The vertical bars at the bottom represent the calculated positions of Bragg diffractions of SmFePO, Sm_2O_3, Fe_2P, and FeP.

(a,c) and atomic positions (z) for the sample in Fig. 2 that were obtained from the Rietveld refinement (R_{wp}=8.23%) (Ref. 26) are a=3.880 69(5), c=8.2054(1), and z =0.14 502(9) for Sm, and z=0.6423(4) for P. The lattice parameters exhibit a large scatter (a=0.3878 ± 0.0004 nm and c=0.8206 ± 0.0004 nm) among samples prepared by similar procedures. The scattering presumably results from the compositional variation or nonstoichiometry of the samples. Variations in the lattice constants lead to a change in T_c, which is discussed in Sec. IV.

B. Electrical properties

Figure 3 shows temperature (T) dependence of ρ for six samples. The inset shows expanded ρ–T curves of a

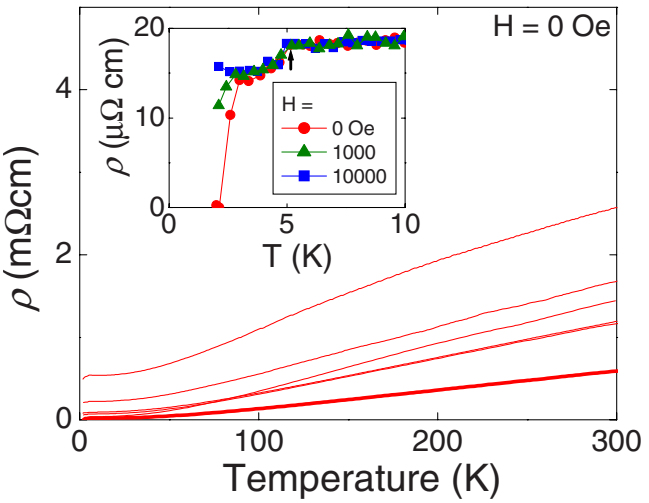

FIG. 3. (Color online) Temperature (T) dependence of electrical resistivities (ρ) for SmFePO under a magnetic field (H) of 0 Oe. The bold ρ–T curve corresponds to the lowest-ρ sample. The inset shows ρ–T curves for the lowest-ρ sample under H=0, 1000, and 10 000 Oe below 10 K. The arrow indicates a kink in the curve.

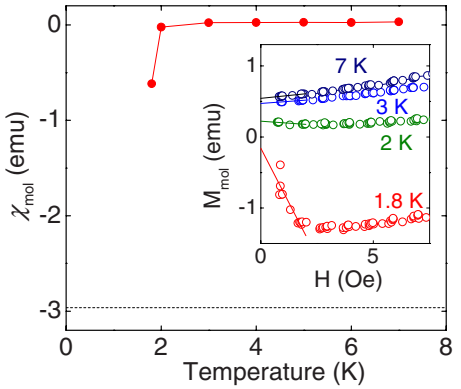

FIG. 4. (Color online) Molar magnetic susceptibility (χ_{mol}) of the lowest-ρ sample of SmFePO as a function of temperature. The value of χ_{mol} was obtained from the slope of a straight-line fit in the inset. The dotted line denotes the perfect diamagnetism (χ_{mol} =−2.96 emu) for SmFePO. The inset shows molar magnetization (M_{mol}) versus magnetic field (H).

SmFePO sample that shows the lowest ρ under several magnetic fields at temperatures below 10 K. All the samples show metallic conduction in the normal conducting state. As seen in the inset, ρ of the lowest-ρ SmFePO shows a sharp decrease with T and becomes zero below 2 K, whereas the other samples do not exhibit zero resistivity, which is due to the superconducting transition and is confirmed by the magnetization measurement (Sec. III C). T_c is defined as a temperature where ρ is half of that at 6 K ($\rho_{6\ K}$). A discontinuous drop (kink) is observed in the $\rho-T$ curve around 5 K, indicated by an arrow in the inset. The kink temperature is almost insensitive to applied magnetic field (H) while T_c decreases with the increasing field strength.

C. Magnetic properties

Figure 4 shows T dependence of the molar magnetic susceptibility (χ_{mol}) for the lowest-ρ SmFePO. The inset shows magnetization (M_{mol}) versus magnetic-field (H) curves for several temperatures from 1.8 to 7 K. The χ_{mol} values are obtained from a linear fit in low H ($H<2$ Oe). χ_{mol} reaches about 20% of the perfect diamagnetic susceptibility, which substantiates the bulk superconductivity of SmFePO. Figure 5 shows temperature dependence of M_{mol}/H under a fixed magnetic field of 10 000 Oe from 2 to 300 K. M_{mol}/H is practically equal to χ_{mol} in this temperature region because a linear $M_{mol}-H$ relation is observed. The χ_{mol} values are of the order of 10^{-3} emu showing a maximum at $T=\sim 5$ K. The maximum is probably due to a magnetic transition (T_N) from paramagnetic to antiferromagnetic phases. We decomposed the $\chi_{mol}-T$ curve from 5 to 300 K into two components: a Curie-Weiss term $[C/(T-\theta)]$ and a weakly temperature-dependent paramagnetic term, which is composed of Pauli paramagnetism,[31] van Vleck paramagnetism, and core electron diamagnetism. The Curie-Weiss term, shown by the red curve in the lower part of the figure, is plotted as the Curie-Weiss relationship in the inset. An apparent magnetic moment is calculated to be $0.37\mu_B$/Sm from the slope, which is in accordance with that of the Sm^{3+} ion.[32]

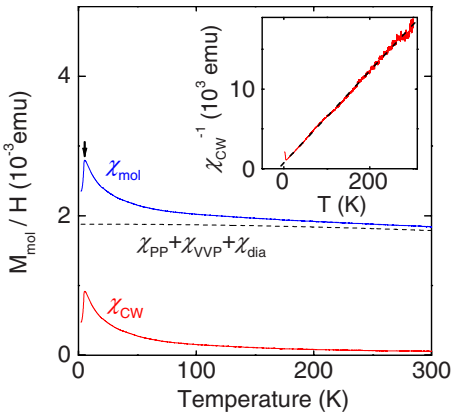

FIG. 5. (Color online) Molar magnetic susceptibility ($\chi_{mol}=M_{mol}/H$) as a function of temperature (T) measured. Measurements were performed at a fixed magnetic field (H) of 10 000 Oe(blue line). Ferromagnetic impurity-free sample is employed. The blue curve is decomposed into the temperature sensitive Curie-Weiss (χ_{CW}) term and the slightly sensitive term, which originated from the Pauli paramagnetism (χ_{PP}), van Vleck paramagnetism (χ_{VVP}), and the core electron diamagnetism (χ_{dia}). $\chi_{PP}+\chi_{VVP}+\chi_{dia}$ may be provided by $\chi_0(1+cT^2)$, ($\chi_0=1.88\times10^{-3}$ emu/mol, $c=-5.50\times10^{-7}/K^2$). The inset shows the Curie-Weiss plot of χ_{CW}.

D. ^{57}Fe Mössbauer spectroscopy

Figure 6 shows ^{57}Fe Mössbauer spectra of SmFePO at temperatures from 298 to 2.2 K. Each spectrum appears to be dominated by a singlet pattern although several weak peaks, indicated by arrows in the figure, are observed at 2.2 K. The weak peaks may be attributed to the magnetic impurity

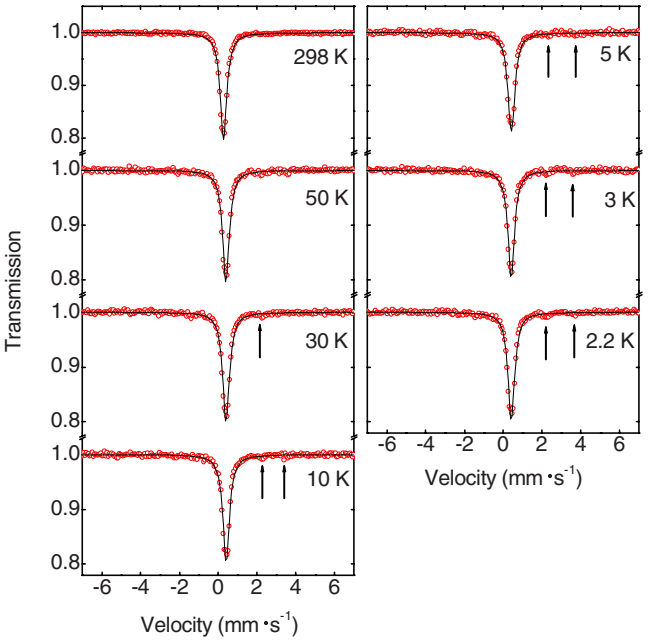

FIG. 6. (Color online) ^{57}Fe Mössbauer spectra (open circle) of SmFePO. Measured temperatures were described in the figure. Solid lines show the fitted singlet patterns. Arrows indicate minor peaks arising from a magnetic splitting due to impurity phases.

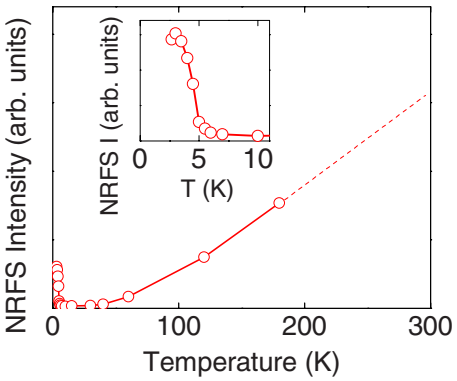

FIG. 7. (Color online) Temperature (T) dependence of the NRFS intensity (I) of ^{149}Sm in SmFePO. The inset shows an expanded graph below 10 K.

phases.[33] The singlet patterns, where internal magnetic fields ($H_{\rm int}$) of Fe are too weak to be detected, indicate that the magnetic moments are quenched. On the other hand, the isomer-shift value is 0.28 mm/s at 298 K, which is almost equal to that of the undoped LaFePO.[34]

E. ^{149}Sm nuclear resonant forward-scattering spectroscopes

Figure 7 shows temperature dependence of the delayed NRFS intensity of ^{149}Sm of the superconducting SmFePO. The NRFS intensity shows a minimum at ~5 K, which increases rapidly with a further decrease in temperature. The minimum is a result of the appearance of a hyperfine magnetic field[35] and can be attributed to the antiferromagnetic ordering of the magnetic moments of Sm^{3+} in SmFePO because the temperature of the minimum agrees with T_N.

Figure 8 shows time-resolved spectra of the NRFS intensity at 150 and 3 K. The spectrum at 150 K consists mainly of a "dynamical beat[24]" related to the effective thickness of the sample with a small quadrupole splitting component. On the other hand, in the spectrum at 3 K, a complex structure superposing on the dynamical beat was observed. The structure can be attributed to a "quantum beat," which results from the hyperfine splitting of Sm nuclear ground and excited states. The splitting is mainly due to $H_{\rm int}$ produced by Sm electronic states.[24,36] $H_{\rm int}$ of Sm was evaluated to be 351.5(3) tesla at 3 K. Thus, the existence of the quantum beat gives a direct evidence for magnetic ordering of Sm^{3+}. Together with the observation of the $\chi_{\rm mol}$ maximum in the $\chi_{\rm mol}-T$ curves at ~5 K, it leads to the conclusion that the magnetic moments of Sm ions order antiferromagnetically below $T=5$ K. Assuming that the magnetic exchange and crystal field are negligible compared to the spin-orbit interaction, the magnetic moment was estimated to be $\sim 0.74\mu_B/\mathrm{Sm}$.[37] The value is larger than that obtained using the Curie-Weiss plot, which was $0.37\mu_B/\mathrm{Sm}$. This discrepancy may be ascribed to a magnetic screening due to the combined effects of the crystalline field and magnetic exchange effects.

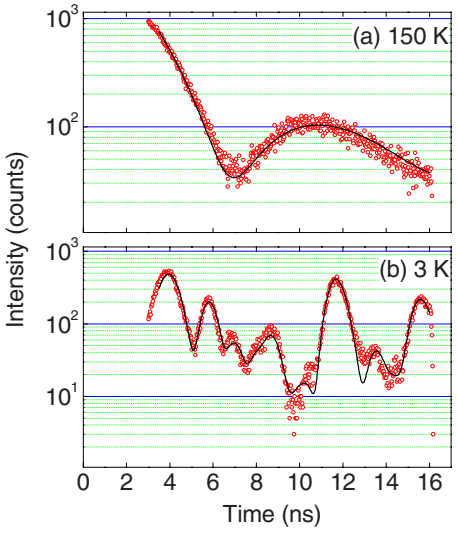

FIG. 8. (Color online) Time resolved spectra of the nuclear resonant forward scattering emitted from ^{149}Sm in SmFePO. The spectra are measured at (a) 150 and (b) 3 K.

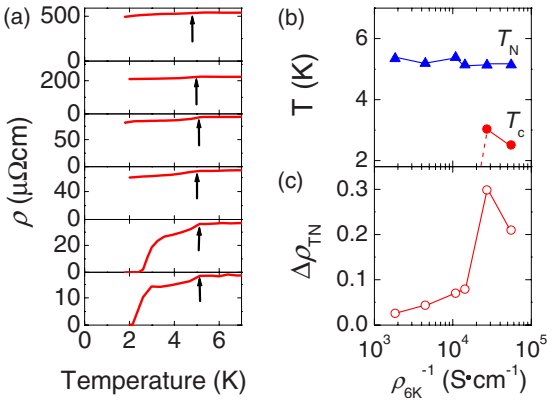

FIG. 9. (Color online) (a) Expanded graph of the $\rho-T$ curves in Fig. 3 below 7 K. T_N is indicated by an arrow. (b) T_c (red closed circles) and T_N (blue closed triangle) versus electrical conductivity at 6 K ($1/\rho_{6\ \mathrm{K}}$). (c) A resistivity decrease $[\Delta\rho_{T_N}=(\rho_{6\ \mathrm{K}}-\rho_{4\ \mathrm{K}})/\rho_{4\ \mathrm{K}}]$ around T_N as a function of the $1/\rho_{6\ \mathrm{K}}$.

IV. DISCUSSION

We discuss the possible factors that influence T_c using the electrical conductivity and lattice constants. Figure 9(a) shows the expanded $\rho-T$ curves below 7 K, where temperatures of discontinuous drops being accompanied with T_N are shown by arrows. Only two samples show the superconducting transition at ~3 K, and the electrical resistivity at 6 K ($\rho_{6\ \mathrm{K}}$) changes widely among the samples from 18 to 542 $\mu\Omega$ cm, whereas the variation in T_N is relatively small.

To clearly demonstrate this view, the T_c and T_N values of the SmFePO samples are plotted against $1/\rho_{6\ \mathrm{K}}$ in Fig. 9(b). It is further observed that only samples with conductivity $>2\times10^4$ S cm undergo superconducting transitions above 1.8 K. A similar character was observed in undoped LaFePO.[25] The amounts by which the resistivity decreases at the kink temperature (i.e., T_N of Sm^{3+}) are also plotted as a function of $1/\rho_{6\ \mathrm{K}}$ in Fig. 9(c). $\Delta\rho_{TN}$ behaves similarly to T_c against $1/\rho_{6\ \mathrm{K}}$, implying whether the carrier density or car-

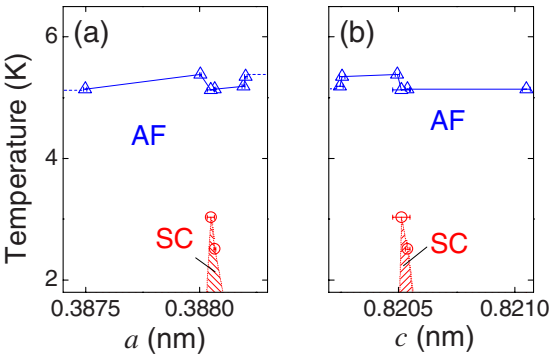

FIG. 10. (Color online) T_c (red closed circles) and T_N (blue open triangles) versus lattice constants (a) a and (b) c axes with the statistical errors for SmFePO. Solid and dotted lines are visual guides for antiferromagnetic phase (AF) . The superconducting phase (SC) appears in a limited narrow area designated by the red shadow.

rier mobility is the dominant factor for controlling $\Delta\rho_{TN}$. $\Delta\rho_{TN}$ is probably equal to the strength of the finite magnetic interaction between conducting carriers and the magnetic moments of Ln ions. The finite magnetic interaction is raising T_c instead of lowering it.

Finally, we discuss the relationship of T_N and T_c with the lattice constants. Figure 10 shows the T_c values of the samples as a function of the lattice constants. Differences in the lattice parameters must represent some differences in composition or stoichiometry of the SmFePO. Although the lattice constants were scattered among the samples, the superconducting samples show very small scattering in the lattice constants (a=0.3880 nm and c=0.8205 nm). T_c in the undoped SmFePO appears in a narrow region of lattice constants with an optimum conductivity. On the other hand, the lattice constants have a little influence on T_N.

V. CONCLUSIONS

SmFePO exhibits T_c below ~3 K and T_N at ~5 K, indicating the coexistence of magnetic and superconducting phases below ~3 K. T_c decreases sharply with a variation in the lattice constants among the samples, whereas T_N is insensitive to the variation.

Resistivity shows a discontinuous decrease around T_N, indicating that a finite magnetic interaction exists between carriers and the magnetic moments of Ln ions. The degree of the decrease is well correlated with the variation in T_c.

^{57}Fe Mössbauer spectra verify that the magnetic moment of Fe is almost quenched in the range of 2.2–298 K. On the other hand, the magnetic moment of Sm is estimated to be $0.37\mu_B$ from the Curie-Weiss fitting, while a value of $0.74\mu_B$ is obtained in the antiferromagnetic phase from the time spectra of the NRFS emitted from ^{149}Sm.

ACKNOWLEDGMENT

We thank Yoshio Kobayashi in RIKEN for his help in the measurements and discussions.

*Present address: Japan Science and Technology Agency, TRiP, Materials and Structures Laboratory, Tokyo Institute of Technology, Mail Box S2-13, 4259 Nagatsuta, Midori-ku, Yokohama 226-8503, Japan.

[1] B. T. Matthias, H. Suhl, and E. Corenzwit, Phys. Rev. Lett. **1**, 92 (1958).

[2] For a review, see H. F. Braun, M. Deroux, B. D. Dunlap, Ø. Fischer, F. Y. Fradin, A. J. Freeman, P. Fulde, H. C. Hamaker, M. Ishikawa, T. Jarlborg, D. C. Johnston, J. Keller, C. W. Kimball, J. W. Lynn,M. B. Maple, D. E. Moncton, J. Muller, G. K. Shenoy, G. Shirane, W. Thomlinson, and L. D. Woolf, *Superconductivity in Ternary Compounds II, Topics in Current Physics*, edited by Ø. Fischer and M. B. Mapple (Springer-Verlag, Berlin, 1982).

[3] Ø. Fischer, A. Treyvaud, R. Chevrel, and M. Sergent, Solid State Commun. **17**, 721 (1975); M. Ishikawa and Ø. Fischer, *ibid.* **24**, 747 (1977); J. W. Lynn, G. Shirane, W. Thomlinson, and R. N. Shelton, Phys. Rev. Lett. **46**, 368 (1981).

[4] B. T. Matthias, E. Corenzwit, J. M. Vandenberg, and H. Barz, Proc. Natl. Acad. Sci. U.S.A. **74**, 1334 (1977); J. M. Vandenberg and B. T. Matthias, *ibid.* **74**, 1336 (1977); H. C. Hamaker, L. D. Woolf, H. B. MacKay, Z. Fisk, and M. B. Maple, Solid State Commun. **31**, 139 (1979).

[5] R. J. Cava, H. Takagi, H. W. Zandbergen, J. J. Krajewski, W. F. Peck, Jr., T. Siegrist, B. Batlogg, R. B. van Dover, R. J. Felder, K. Mizuhashi, J. O. Lee, H. Eisaki, and S. Uchida, Nature (London) **367**, 252 (1994); H. Eisaki, H. Takagi, R. J. Cava, B. Batlogg, J. J. Krajewski, W. F. Peck, K. Mizuhashi, J. O. Lee, and S. Uchida, Phys. Rev. B **50**, 647 (1994); J. W. Lynn, S. Skanthakumar, Q. Huang, S. K. Sinha, Z. Hossain, L. C. Gupta, R. Nagarajan, and C. Godart, *ibid.* **55**, 6584 (1997).

[6] I. Shirotani, T. Uchiumi, K. Ohno, C. Sekine, Y. Nakazawa, K. Kanoda, S. Todo, and T. Yagi, Phys. Rev. B **56**, 7866 (1997); T. Namiki, Y. Aoki, H. Sato, C. Sekine, I. Shirotani, T. D. Matsuda, Y. Haga, and T. Yagi, J. Phys. Soc. Jpn. **76**, 093704 (2007).

[7] M. K. Wu, J. R. Ashburn, C. J. Torng, P. H. Hor, R. L. Meng, L. Gao, Z. J. Huang, Y. Q. Wang, and C. W. Chu, Phys. Rev. Lett. **58**, 908 (1987); P. H. Hor, R. L. Meng, Y. Q. Wang, L. Gao, Z. J. Huang, J. Bechtold, K. Forster, and C. W. Chu, *ibid.* **58**, 1891 (1987); see, for example, P. Fischer, B. Schmid, P. Brüesch, F. Stucki, and P. Unternährer, Z. Phys. B: Condens. Matter **74**, 183 (1989); K. N. Yang, J. M. Ferreira, B. W. Lee, M. B. Maple, W. H. Li, J. W. Lynn, and R. W. Erwin, Phys. Rev. B **40**, 10963 (1989), and references cited therein.

[8] Y. Tokura, H. Takagi, and S. Uchida, Nature (London) **337**, 345 (1989); J. W. Lynn, I. W. Sumarlin, S. Skanthakumar, W. H. Li, R. N. Shelton, J. L. Peng, Z. Fisk, and S. W. Cheong, Phys. Rev. B **41**, 2569 (1990); I. W. Sumarlin, S. Skanthakumar, J. W. Lynn, J. L. Peng, Z. Y. Li, W. Jiang, and R. L. Greene, Phys. Rev. Lett. **68**, 2228 (1992).

[9] Y. Kamihara, H. Hiramatsu, M. Hirano, R. Kawamura, H. Yanagi, T. Kamiya, and H. Hosono, J. Am. Chem. Soc. **128**,

10012 (2006).
[10] Y. Kamihara, T. Watanabe, M. Hirano, and H. Hosono, J. Am. Chem. Soc. **130**, 3296 (2008).
[11] H. Takahashi, K. Igawa, K. Arii, Y. Kamihara, M. Hirano, and H. Hosono, Nature (London) **453**, 376 (2008).
[12] X. H. Chen, T. Wu, G. Wu, R. H. Liu, H. Chen, and D. F. Fang, Nature (London) **453**, 761 (2008); Z. A. Ren, W. Lu, J. Yang, W. Yi, X. L. Shen, Z. C. Li, G. C. Che, X. L. Dong, L. L. Sun, F. Zhou, and Z. X. Zhao, Chin. Phys. Lett. **25**, 2215 (2008).
[13] Z. A. Ren, G. C. Che, X. L. Dong, J. Yang, W. Lu, W. Yi, X. L. Shen, Z. C. Li, L. L. Sun, F. Zhou, and Z. X. Zhao, Europhys. Lett. **83**, 17002 (2008); H. Kito, H. Eisaki, and A. Iyo, J. Phys. Soc. Jpn. **77**, 063707 (2008).
[14] $CeO_{1-x}F_xFeAs$: G. F. Chen, Z. Li, D. Wu, G. Li, W. Z. Hu, J. Dong, P. Zheng, J. L. Luo, and N. L. Wang, Phys. Rev. Lett. **100**, 247002 (2008); Z. A. Ren, J. Yang, W. Lu, W. Yi, G. C. Che, X. L. Dong, L. L. Sun, and Z. X. Zhao, Mater. Res. Innovations **12**, 105 (2008); P. Cheng, L. Fang, H. Yang, X. Y. Zhu, G. Mu, H. Q. Luo, Z. S. Wang, and H. H. Wen, Sci. China, Ser. G **51**, 719 (2008); J. W. G. Bos, G. B. S. Penny, J. A. Rodgers, D. A. Sokolov, A. D. Huxley, and J. P. Attfield, Chem. Commun. (Cambridge) **2008**, 3634; C. Wang, L. Li, S. Chi, Z. Zhu, Z. Ren, Y. Li, Y. Wang, X. Lin, Y. Luo, S. Jiang, X. Xu, G. Cao, and Z. Xu, Europhys. Lett. **83**, 67006 (2008).
[15] B. I. Zimmer, W. Jeitschko, J. H. Albering, R. Glaum, and M. Reehuis, J. Alloys Compd. **229**, 238 (1995).
[16] P. Quebe, L. J. Terbuchte, and W. Jeitschko, J. Alloys Compd. **302**, 70 (2000).
[17] L. Ding, C. He, J. K. Dong, T. Wu, R. H. Liu, X. H. Chen, and S. Y. Li, Phys. Rev. B **77**, 180510 (2008); Y. Qiu, Wei Bao, Q. Huang, T. Yildirim, J. Simmons, J. W. Lynn, Y. C. Gasparovic, J. Li, M. Green, T. Wu, G. Wu, and X. H. Chen, arXiv:0806.2195 (unpublished); J. Zhao, Q. Huang, C. de la Cruz, S. Li, J. W. Lynn, Y. Chen, M. A. Green, G. F. Chen, G. Li, Z. Li, J. L. Luo, N. L. Wang, and P. Dai, arXiv:0806.2528, Nature Mater. (to be published); A. Martinelli, M. Ferretti, P. Manfrinetti, A. Palenzona, M. Tropeano, M. R. Cimberle, C. Ferdeghini, R. Valle, M. Putti, and A. S. Siri, Supercond. Sci. Technol. **21**, 095017 (2008); R. Cimberle, C. Ferdeghini, F. Canepa, M. Ferretti, A. Martinelli, A. Palenzona, A. S. Siri, and M. Tropeano, arXiv:0807.1688 (unpublished).
[18] S. Ishibashi, K. Terakura, and H. Hosono, J. Phys. Soc. Jpn. **77**, 053709 (2008); H. Fukuyama, JPSJ Online-News and Comments, 12 May 2008.
[19] T. Nomura, S. W. Kim, Y. Kamihara, M. Hirano, P. V. Sushko, K. Kato, M. Takata, A. L. Shluger, and H. Hosono, arXiv:0804.3569, Supercond. Sci. Technol. (to be published); C. de la Cruz, Q. Huang, J. W. Lynn, Jiying Li, W. Ratcliff II, J. L. Zarestky, H. A. Mook, G. F. Chen, J. L. Luo, N. L. Wang, and P. Dai, Nature (London) **453**, 899 (2008).
[20] S. Kitao, Y. Kobayashi, S. Higashitaniguchi, M. Saito, Y. Kamihara, M. Hirano, T. Mitsui, H. Hosono, and M. Seto, J. Phys. Soc. Jpn. **77**, 103706 (2008).
[21] C. H. Lee, A. Iyo, H. Eisaki, H. Kito, M. T. Fernandez-Diaz, T. Ito, K. Kihou, H. Matsuhata, M. Braden, and K. Yamada, J. Phys. Soc. Jpn. **77**, 083704 (2008).
[22] R. L. Mössbauer, Z. Phys. **151**, 124 (1958) (in German).
[23] J. B. Hastings, D. P. Siddons, U. van Bürck, R. Hollatz, and U. Bergmann, Phys. Rev. Lett. **66**, 770 (1991).
[24] G. V. Smirnov, Hyperfine Interact. **123-124**, 31 (1999).
[25] Y. Kamihara, M. Hirano, H. Yanagi, T. Kamiya, Y. Saitoh, E. Ikenaga, K. Kobayashi, and H. Hosono, Phys. Rev. B **77**, 214515 (2008).
[26] TOPAS, version 3; Bruker AXS: Karlsruhe Germany, 2005.
[27] Y. V. Shvydko, Phys. Rev. B **59**, 9132 (1999); Hyperfine Interact. **125**, 173 (2000).
[28] D. Bellavance, M. Vlasse, B. Morris, and A. Wold, J. Solid State Chem. **1**, 82 (1969).
[29] H. Fujii, T. Hōkabe, T. Kamigaichi, and T. Okamoto, J. Phys. Soc. Jpn. **43**, 41 (1974).
[30] J. H. Van Vleck, *Theory of Electric and Magnetic Susceptibilities* (Oxford University Press, New York, 1932).
[31] N. F. Mott and H. Jones, *The Theory of the Properties of Metals and Alloys* (Clarendon, Oxford, 1936).
[32] J. Llanos, R. Cortés, T. Guizouarn, and O. Peña, Mater. Res. Bull. **41**, 1266 (2006).
[33] The minor peaks observed in Fig. 6 may be explained by the minor magnetic ordered components indicating $H_{\mathrm{int}} = 10-20$ tesla. Total fraction of the magnetic components is less than 12 vol %.
[34] IS=0.13, reported by Y. Kobayashi, Y. Kamihara, M. Hirano, and H. Hosono (unpublished); M. Tegel, I. Schellenberg, R. Pöttgen, and D. Johrendt, Z. Naturforsch., B: Chem. Sci. **63**, 1057 (2008).
[35] The increase in the recoil-free fraction, which corresponds to the increase in effective thickness with decreasing temperature, induces acceleration of the time decay of the excited state (Ref. 24). This effect is called the speed-up effect. Therefore, if we do not measure the time spectrum from the time prompt synchrotron-radiation pulse that excited the nucleus, an increase in the effective thickness (recoil-free fraction) sometimes causes a decrease in the "delayed intensity." To avoid the effects of a strong prompt synchrotron-radiation pulse, delayed components were measured from 3 ns after the pulse in our measurement. As shown in Fig. 8, the delayed intensity decreases as the temperature is lowered to T_N although this is contrary to what is expected from the increase in the recoil-free fraction. However, the appearance of the hyperfine splitting decreases the effective thickness for the degenerated state, explaining the observed increase in the delayed intensity as the hyperfine splitting increases below T_N.
[36] S. Tsutsui, Y. Kobayashi, Y. Yoda, M. Seto, K. Indoh, and H. Onodera, J. Magn. Magn. Mater. **272-276**, 199 (2004).
[37] Provided that the magnetic moment of an ion is proportional to the internal magnetic field (H_{int}), the conversion factor (CF) is defined by the relation between the ion's magnetic moment (μ) and internal magnetic field (H_{int}) using the Lande g factor (g_{Lande}) and the total angular-momentum quantum number (J): $\mu/\mu_{\mathrm{B}} = g_{\mathrm{Lande}} J \equiv |H_{\mathrm{int}}/\mathrm{CF}|$. On the other hand, H_{int} of a rare-earth ion is obtained from the relationship using the magnetic hyperfine splitting constant (JA) and nuclear g factor (g_n); (S1) B. Bleaney, in *Magnetic Properties of Rare-Earth Metals*, edited by R. J. Elliott (Plenum, New York, 1972), p. 394; as follows: $-H_{\mathrm{int}} = \frac{(JA)(10^6\ \mathrm{Hz})}{762.28 g_n}(10^6\ \mathrm{G})$. The equation transforms into $J = \frac{762.28 g_n}{A} H_{\mathrm{int}}$. JA of ^{149}Sm is calculated as −495, which is converted from the JA of ^{147}Sm (=−600$^{(S1)}$) using a ratio of dipole interaction constants A^{147}/A^{149} (=1.21302); (S2) G. K. Woodgate, Proc. R. Soc. London, Ser. A **293**, 117 (1966); Then, A is calculated as −197.86 using $J=5/2$ for Sm^{3+} ($4f^5 5s^2 p^6$). g_n is calculated as −0.191 using a nuclear magnetic moment of ^{149}Sm

($-0.6677\mu_n$) and a nuclear-spin quantum number of ^{149}Sm (7/2). (*S*3) http://ie.lbl.gov/ensdf/; J. G. England, I. S. Grant, J. A. R. Griffith, D. E. Evans, D. A. Eastham, G. W. A. Newton, and P. M. Walker, J. Phys. G **16**, 105 (1990); μ_n denotes nuclear magneton. Therefore, 476 tesla/μ_B is adapted for the CF of $^{149}Sm^{3+}$ using the following equation: $CF \equiv \frac{H_{int}}{g_{Lande}J} = \frac{A}{762.28 g_{Lande} g_n}$ $\cong 4.76(10^6\ G/\mu_B) = 476\ (tesla/\mu_B)$. This value is the same as that obtained by Barla *et al.*; (S4) A. Barla, J. P. Sanchez, Y. Haga, G. Lapertot, B. P. Doyle, O. Leupold, R. Rüffer, M. M. Abd-Elmeguid, R. Lengsdorf, and J. Flouquet, Phys. Rev. Lett. **92**, 066401 (2004).